iScience

CellPress

Article

Self-Enhanced Carbonized Polymer Dots for Selective Visualization of Lysosomes and Real-Time Apoptosis Monitoring

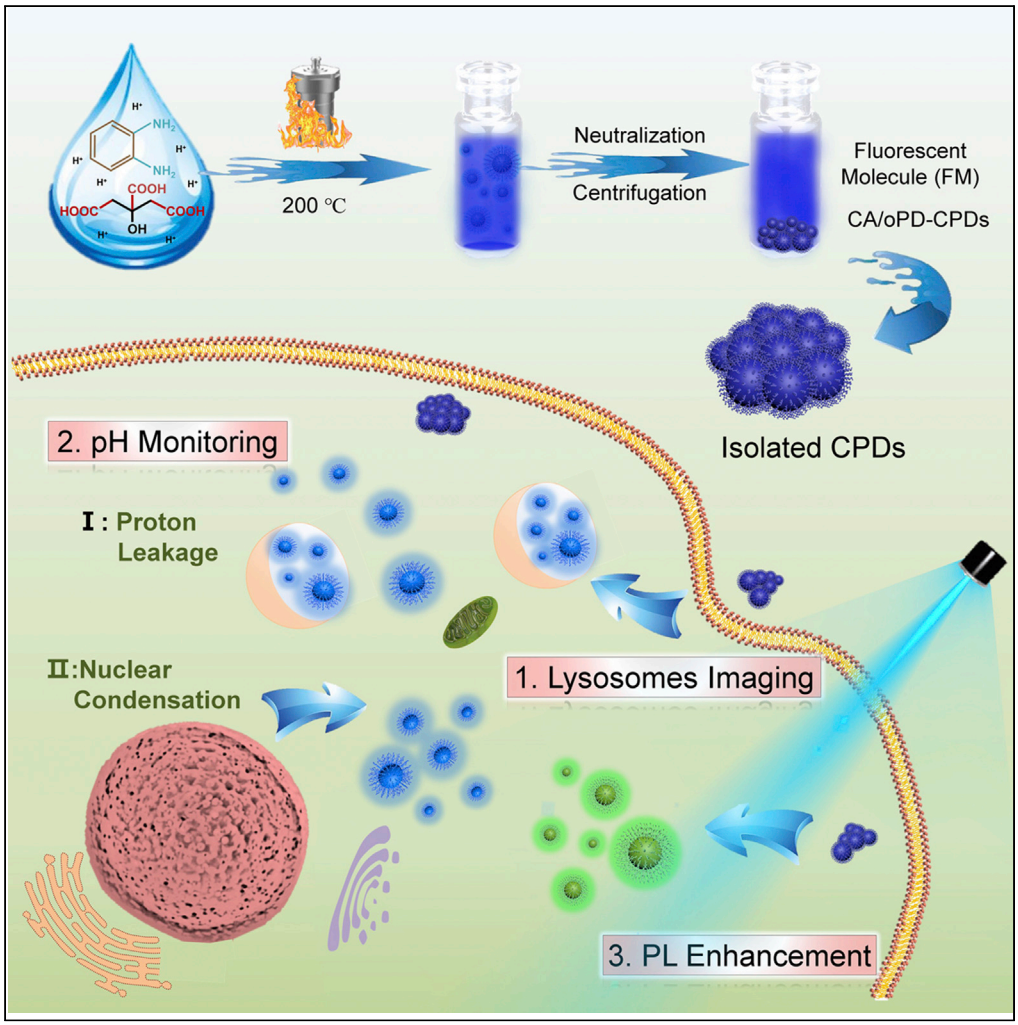

Xiaohuan Zhao, Jing Li, Dongning Liu, Mingxi Yang, Wenjing Wang, Shoujun Zhu, Bai Yang

byangchem@jlu.edu.cn

HIGHLIGHTS

CA/oPD-CPDs with extreme pH sensitivity through aggregation-dissociation process

Irradiation-enhanced CA/oPD-CPDs for mapping living cells in a real-time manner

CA/oPD-CPDs super-nanoparticles assembly to selectively visualize lysosomes

Mapping the spatial distribution of pH in living cells during apoptosis

Zhao et al., iScience *23*, 100982
April 24, 2020
https://doi.org/10.1016/j.isci.2020.100982

iScience

CellPress

Article

Self-Enhanced Carbonized Polymer Dots for Selective Visualization of Lysosomes and Real-Time Apoptosis Monitoring

Xiaohuan Zhao,[1] Jing Li,[2] Dongning Liu,[3] Mingxi Yang,[1] Wenjing Wang,[1] Shoujun Zhu,[1,4] and Bai Yang[1,5,*]

SUMMARY

Protons are highly related to cell viability during physiological and pathological processes. Developing new probes to monitor the pH variation could be extremely helpful to understand the viability of cells and the cell death study. Carbonized polymer dots (CPDs) are superior biocompatible and have been widely applied in bioimaging field. Herein, a new type of extreme-pH suitable CPDs was prepared from citric acid and o-phenylenediamine (CA/oPD-CPDs). Due to the co-existence of hydrophilic and hydrophobic groups, CA/oPD-CPDs tend to aggregate in neutral condition with a dramatic decrease of fluorescence, but disperse well in both acidic and alkaline conditions with brighter emission. This specialty enables them to selectively illuminate lysosomes in cells. Moreover, CA/oPD-CPDs in the cytoplasm could serve as a sustained probe to record intracellular pH variation during apoptosis. Furthermore, CA/oPD-CPDs present a continuous fluorescence increase upon 2-h laser irradiation in living cells, underscoring this imaging system for long-term biological recording.

INTRODUCTION

Protons play crucial roles in living cells during physiological and pathological processes, including intracellular protein degradation in lysosomes, homeostasis, and cell death (Gottlieb et al., 1995, 1996; Zanke et al., 1998). Acidification is an early feature of apoptosis and cell death. The sets of proteins-enzymes related to apoptosis exclusively operate at acidic pH values. Monitoring the acidification of living cells is thus a universal approach to identify cell viability and measure the efficiency of anti-cancer drugs. To satisfy this need, the materials need to be biocompatible and able to remain in the living cells without being digested within a long period. However, some organic dyes are unable to function in acid circumstances and easily digested within hours in living cells. Thus, there is an ever-increasing demand for developing pH-responsive and extreme-pH-suitable fluorescence materials that are non-toxic and can be permanently preserved in living cells.

Compared with traditional semiconductor quantum dots (Chen et al., 2015), fluorescent carbon dots (CDs) have drawn great attentions (Baker and Baker, 2010; Yang et al., 2013; Zhang et al., 2012) due to their good biocompatibility, chemical stability, easy chemical modification, and low toxicity (Cao et al., 2013; Li et al., 2012), holding promising for use in various fields including the bioimaging (Du et al., 2019; Zhao et al., 2019; Zheng et al., 2015), optical sensing (Dong et al., 2015; Zhang et al., 2014; Zhao et al., 2015), medical diagnosis (Kong et al., 2012), catalysis (Jin et al., 2015; Li et al., 2010), and photovoltaic devices (Gupta et al., 2011). Notably, CDs can be obtained from many materials, such as polymer (Liu et al., 2012), amino acid (Jiang et al., 2012; Lu et al., 2014), protein (Liu et al., 2013), sugar (Yang et al., 2011), and some small molecules such as citric acid (Liu et al., 2013; Qu et al., 2012, 2014b; Zhai et al., 2012; Zhu et al., 2013), which are highly abundant on the earth. However, due to the variety of CDs, the photoluminescence (PL) mechanism and the classification of CDs are still open debates (Cayuela et al., 2016; Xia et al., 2019; Zhu et al., 2015). Generally, they can be divided into three types, including graphene quantum dots (GQDs), carbon quantum dots (CQDs), and carbon nanodots (CNDs) (Cayuela et al., 2016). Notably, those CDs from small molecules always suffered an uncompleted carbonization process, including sequential polymerization, dehydration, and carbonization. The resulting CDs consist of polymeric structures or polymer/carbon hybrid structures, reasonably regarded as carbonized polymer dots (CPDs) (Xia et al., 2019). CPDs from small molecules always contain neglected fluorescent molecules, which have been confirmed by several papers (Kasprzyk et al., 2013, 2015; Krysmann et al., 2012; Song et al., 2015; Zhu et al., 2016). Heretofore, efficient separation of

[1]State Key Laboratory of Supramolecular Structure and Materials, College of Chemistry, Jilin University, Changchun, Jilin 130012, P. R. China

[2]The Scientific Research Center, China-Japan Union Hospital, Jilin University, Changchun, Jilin 130033, P. R. China

[3]Department of Periodontology, Stomatology Hospital, Jilin University, Changchun, Jilin 130021, P. R. China

[4]Key Laboratory of Organ Regeneration & Transplantation of the Ministry of Education, The First Hospital of Jilin University, Changchun, Jilin 130061, P.R. China

[5]Lead Contact

*Correspondence: byangchem@jlu.edu.cn

https://doi.org/10.1016/j.isci.2020.100982

CPDs and small molecule by-products is critical in improving related applications, yet, strategies that completely purify CPDs are always difficult to achieve.

Although CPDs have been widely applied in bioimaging field (Du et al., 2019; Zhao et al., 2019; Zheng et al., 2015), only several papers realized the selective visualization of specific organelles in cells, including nucleolus (Bao et al., 2018; Hua et al., 2018, 2019; Khan et al., 2018), mitochondrion (Gao et al., 2017; Hua et al., 2017), Golgi apparatus (Li et al., 2017; Yuan et al., 2017), and lysosomes (E et al., 2018; Wu et al., 2017; Zhang et al., 2018b). Lysosomes are membrane-bound cytoplasmic organelles, playing critical roles in intracellular macromolecules receiving and degradation from the secretory, endocytic, autophagic, and phagocytic pathways (Saftig and Klumperman, 2009). It is essential to distinguish lysosomes from other organelles, because the improper function of lysosomes will lead to pathological changes, such as lysosomal storage disorders, neurodegenerative diseases, and even cancer (Appelqvist et al., 2013). Different from other organelles, the pH inside of lysosomes is within an acidic range from 3.8 to 6.6 to maintain the function of the degradative enzymes inside lysosomes (Zhang et al., 2018b). Such acid values make lysosomes the most acidic organelles (Cai et al., 2017). Notably, the protons in lysosomes will leak at the early stage of apoptosis, followed by the pH increase in lysosomes and the pH decrease in the cytoplasm (Nilsson et al., 2004). After that, the intracellular pH will further decrease due to the cell nuclear condensation. Consequently, the nucleic acid and the organic acid inside the nucleus are released into the cytoplasm, serving as the indicator for the death of the cell. Nonetheless, CPDs for lysosome visualization and intracellular pH recording are still on the early stage. Yet, only several papers have been published on lysosomes imaging based on CPDs. These CPDs target lysosomes actively and only exist in lysosomes with the need of surface chemistry or afterward surface modification (E et al., 2018; Wu et al., 2017; Zhang et al., 2018b). Although numerous papers described CPDs pH sensors (E et al., 2018; Hu et al., 2014; Lu et al., 2014; Wang et al., 2019; Wu et al., 2014; Zhang et al., 2018b; Zhao et al., 2019; Zhu et al., 2013), most pH-dependent CPDs only present brighter PL emission in neutral aqueous solutions (E et al., 2018; Hu et al., 2014; Wu et al., 2014; Zhang et al., 2018b; Zhu et al., 2013) and are not suitable for acidic environment. Only a few of them possess stronger emission in acid solutions (Lu et al., 2014; Wang et al., 2019; Zhao et al., 2019). The pH sensitivity of CPDs is regarded to result from the protonation and deprotonation of the amino and carboxyl groups on the surface. Among all these papers, only several of them were applied to monitor the pH variation in cells (Wu et al., 2014), and these pH variations in cells entirely came from the buffers with different pH instead of cell metabolism.

As general bioimaging agents, CPDs possess many outstanding properties. They could stain living cells via endocytosis without triggering cell death and perform as a long-lasting imaging probe compared with organic dyes. However, severe photobleaching was found in nearly all reported CPDs and organic dyes, especially with the influence of intracellular acidification and laser irradiation of confocal microscopy. The vulnerability of these bioimaging probes strongly hindered the study of cell death, which demands the bioimaging agent to be stable with both UV light and acid. Although CPDs possess relatively better photostability than organic dyes, the unavoidable fluorescence decay is still detrimental during long-time or repeated laser exposure. Thus, developing a bioimaging agent with neglectable fluorescence loss or even enhanced fluorescence intensity over long-time laser exposure is very meaningful for long-term cell fate monitor.

In this study, we hydrothermally synthesized a new kind of CPDs from citric acid and o-phenylenediamine (named as CA/oPD-CPDs). The synthesis process includes polymerization and further controlled carbonization, forming amorphous carbon nanodots encapsulated by small polymer chains. CA/oPD-CPDs feature aggregation-dissociation adjustable properties and sensitivity to the surrounding pH, owing to the abundance of surface groups, benzene groups, carboxyl groups, and amino groups. Specifically, CA/oPD-CPDs will aggregate in neutral aqueous solution, whereas disperse in both acidic and alkaline circumstances with stable fluorescence. This property allows us to separate CA/oPD-CPDs from molecule by-products entirely via centrifugation and dialysis. After separating the small molecular fluorophore with PLQY as high as 83%, we confirm the pH-dependent PL CPDs with pretty low fluorescence at neutral pH and increased fluorescence under acidic/alkaline conditions. Benefiting from this unconventional pH-sensitive nature of CA/oPD-CPDs, we successfully managed to selectively visualize lysosomes in cells in an unprecedented real-time manner. Different from previous CPDs for lysosome imaging (E et al., 2018; Wu et al., 2017; Zhang et al., 2018b), CA/oPD-CPDs could visualize lysosomes passively regarding the acidic environment in the lysosomes. Without targeting groups, CA/oPD-CPDs possess no selectivity and spread all over

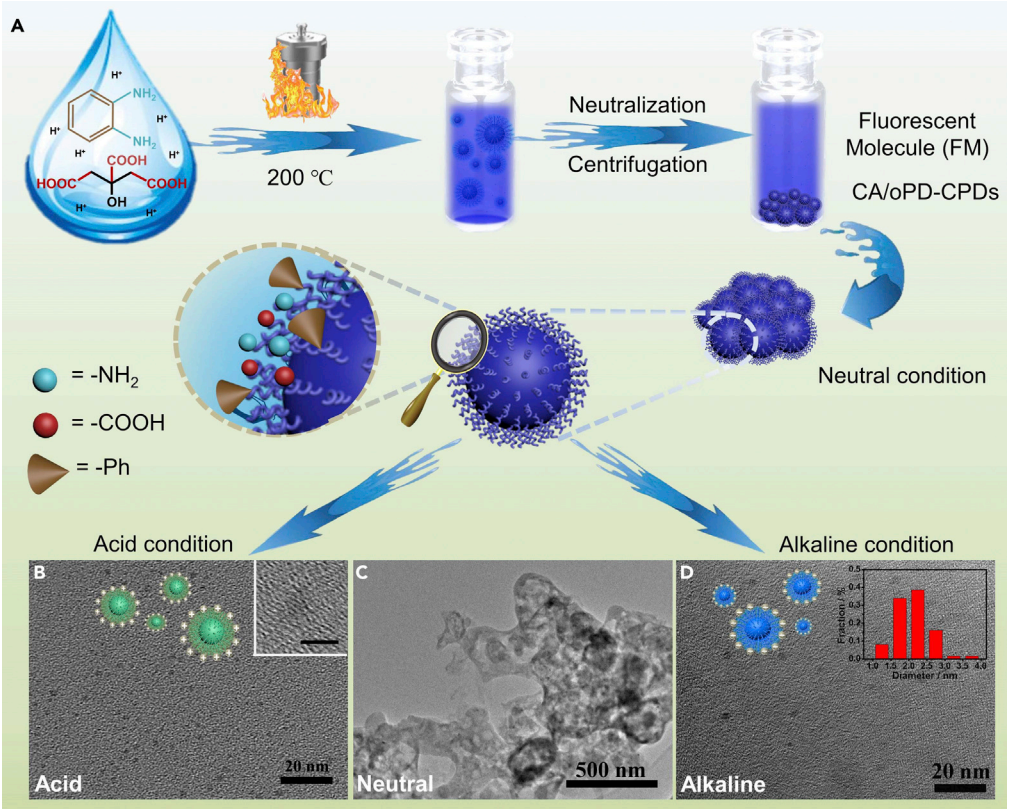

Figure 1. Synthesis and Morphology of CA/oPD-CPDs

(A–D) (A) Preparation routes of fluorescent molecule and CA/oPD-CPDs. Morphology of CA/oPD-CPDs in (B) acid (inset is the high-resolution TEM image of CA/oPD-CPDs with a scale bar of 5 nm), (C) neutral, and (D) alkaline aqueous solutions with either HCl or NaOH (inset is the size distribution of CA/oPD-CPDs).

the cell. Thus, they can also monitor the intracellular pH variation during the apoptosis process, which involves the pH variation in the cytoplasm. Different from other organic dyes or CPDs, which are suffering from photobleaching issue, the as-prepared CA/oPD-CPDs present a continuous fluorescence increase upon 2-h laser irradiation in cells. We confirm the fluorescence enhancement was the result of intracellular acidification. Our investigations identify promising CA/oPD-CPDs are likely essential to cell fate study and can be modulated to improve the identification of the cell viability and the efficiency of anti-cancer drugs.

RESULTS AND DISCUSSION

Preparation and Characterization of Citric Acid/o-Phenylenediamine Carbonized Polymer Dots and the Fluorescent Molecule

The basic procedures to synthesize CA/oPD-CPDs include the decomposition and pyrolysis of citric acid and o-phenylenediamine at 200°C for 8 h. After being neutralized and centrifuged, the supernatant (fluorescent molecule, FM) and sediment (CA/oPD-CPDs) were collected and purified, respectively, as illustrated in Figure 1A. In the UV-vis absorption spectra of FM and CA/oPD-CPDs, peaks at 240 and 277 nm are presumably attributed to π-π* transition, whereas the peak at 302 nm in FM is supposedly the result of n-π* transition of C=O. The wide peak in CA/oPD-CPDs from 300 to 450 nm results from the complex carbon core (Figure S1A). We confirmed the detailed structures of both FM and CA/oPD-CPDs as follows.

We initially investigated the chemical compositions of CA/oPD-CPDs. In the FTIR analysis of CA/oPD-CPDs, the following groups were observed: the stretching vibrations of O-H/N-H at 3,436 cm^{-1} and 3,197 cm^{-1}, the stretching vibrations of C-H at 2,919 cm^{-1}, the peak at 1,643 cm^{-1} assigned to carboxyl (COOH) group, whereas the stretching vibrations of C-N at 1,385 cm^{-1}, the peaks at 1,157 cm^{-1} and 1,076 cm^{-1} corresponded to C-O and N-H groups (Figure S1B) (Bao et al., 2018; Lu et al., 2018). These

functional groups result from reactants and could be further confirmed by X-ray photoelectron spectroscopy (XPS) spectra. The XPS spectra of CA/oPD-CPDs comprised three peaks at 285.0, 400.0, and 532.0 eV, which were attributed to C_{1s}, N_{1s}, and O_{1s}, respectively (Figure S2). The C_{1s} spectrum of CA/oPD-CPDs indicates the presence of three types of carbon bonds: sp^2 carbon (C-C/C=C) at 284.78 eV, sp^3 carbon (C-N/C-O) at 286.3 eV, and oxidized carbon (C=O) at 288.34 eV (Qu et al., 2014a). The N_{1s} spectrum of CA/oPD-CPDs shows two types of N bonds: C-N-C (398.4 eV) and N-$(C)_3$ (400.25 eV) (Qu et al., 2014b). The O_{1s} spectrum of CA/oPD-CPDs shows two types of O bonds: C=O (531.21 eV) and C-OH or C-O-C (533.1 eV) (Feng et al., 2017). Moreover, No D/G band was observed in the Raman spectrum of CA/oPD-CPDs (Figure S3), which further confirmed the amorphous feature of CA/oPD-CPDs. Further more, the elemental composition of CA/oPD-CPDs was measured by elemental analysis, and the elemental content of C 66.97%, H 4.57%, N 15.17%, and O (calculated) 13.29% are provided (Table S1).

Although the existence of benzene groups in CA/oPD-CPDs increased the hydrophobic degree of the whole nanoparticles, the carboxyl groups and amino groups endowed CA/oPD-CPDs with hydrophilic properties in proper pH aqueous solution. As a result, CA/oPD-CPDs are soluble in acid and basic conditions but aggregate in the neutral condition, benefitting the separation of CA/oPD-CPDs from small molecules. As shown in Figure 1D, the diameters of CA/oPD-CPDs were mainly distributed in the range of 1–4 nm with an average diameter of 2.1 nm without lattice structure under high-resolution TEM (inset Figure 1B). At acid or alkaline conditions, CA/oPD-CPDs were either with positive (protonation) or negative (deprotonation) charges and dispersed in the solution as small nanoparticles as shown in Figures 1B and 1D. At neutral condition, the whole CA/oPD-CPDs behave as electrically neutral particles. With the existence of benzene groups, the hydrophobic degree of the whole particles increased and further aggregated in the solution as sediment (Figure 1C). The transformation of CA/oPD-CPDs between well-dispersing nanoparticles and sediment was also illustrated in Figure 1A. Additionally, the hydrophobic groups on CA/oPD-CPDs featured an excellent solubility in organic solvents (Figure S4). The fluorescence intensity increased dramatically compared with that in neutral pH aqueous solution, indicating CA/oPD-CPDs could be well dispersed in the organic phase.

We next aimed to prove the chemical structure of FM. For morphology testing, no nanodots were observed under TEM in FM samples. To analyze the chemical composition of FM, a liquid chromatography-mass spectrometer was used to identify the molecular weight of FM. The main molecular weight was focused on 202, with different retention time. We confirmed that there were a lot of isomerides with the same molecular weight 202, which are the derivative of 1-oxo-1,5-dihydropyrido[1,2-a] benzimidazole-3-carboxylic acid (Figure S5) (Kasprzyk et al., 2015). We also proved that the emission center of CA/oPD-CPDs was covalently FM binding in the CA/oPD-CPDs.

Optical Properties of Citric Acid/o-Phenylenediamine Carbonized Polymer Dots and the Fluorescent Molecule

We then evaluated the fluorescence properties of FM and CA/oPD-CPDs. Because CA/oPD-CPDs and FM are sensitive to pH, the fluorescence spectra of CA/oPD-CPDs and FM at different pH conditions were provided in Figures 2A–2C and S6. The emission peak positions of CA/oPD-CPDs and FM were different at different pH conditions. As depicted in Figure S6, the emission peaks of FM were located at 462, 432, and 460 nm at pH 3, 7, and 12, respectively. Notably, the emission peak presents redshift in both acid and base conditions. Similar to FM, the emission peaks of CA/oPD-CPDs were 482, 450, and 470 nm at pH 2, 7, and 12, respectively. Redshifts were also observed in CA/oPD-CPDs, which further indicates the same fluorescence center in both FM and CA/oPD-CPDs. Noticeably, even though the same fluorescence groups were presumably responsible for the PL origin of both FM and CA/oPD-CPDs, excitation dependent behavior was obviously observed in CA/oPD-CPDs, which was not found in FM. These results indicate that "carbon core" is one of the reasons for excitation dependent behavior. To further analyze this pH-dependent behavior, the fluorescence spectra were analyzed (Figure S7). After normalization, it is clear that the emission peaks shift from greenish to blue region from pH 2 to pH 7 and shift back from pH 7 to pH 12. In this circumstance, redshift was also observed in alkaline conditions (Figure S7). We suppose it could be the result of protonation and reversible chemical reactions, such as keto-enol tautomerism (Figure S8). Notably, this reversible reaction is promoted both in acid and alkaline conditions. The similar fluorescence behavior was also observed in FM (Figure S9).

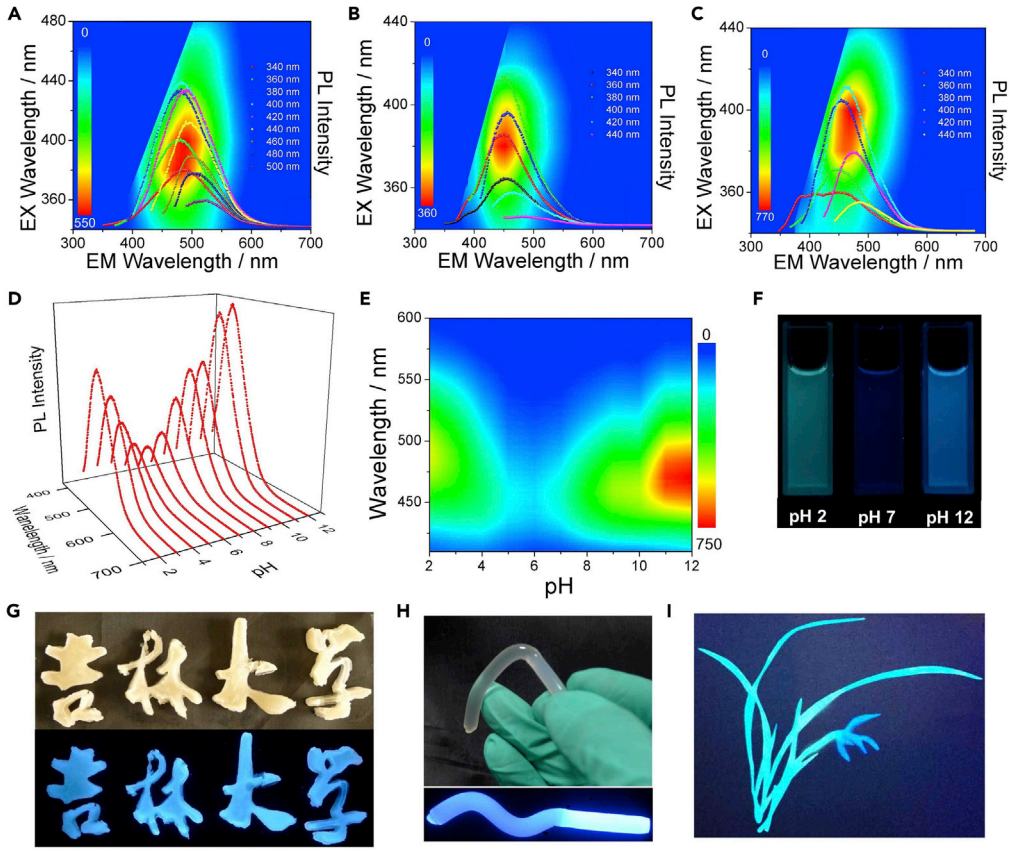

Figure 2. Fluorescence Behavior of CA/oPD-CPDs

(A–C) PL spectra with different excitation wavelengths of CA/oPD-CPDs and corresponding excitation-emission matrix in (A) pH 2, (B) pH 7, and (C) pH 12 aqueous solutions with either HCl or NaOH.

(D) The PL spectra of CA/oPD-CPDs excited with 380 nm at different pH values.

(E) Emission-pH matrix of the same concentration CA/oPD-CPDs aqueous solution with different pH.

(F) Digital photos of CA/oPD-CPDs in pH 2, pH 7, and pH 12 aqueous solutions with either HCl or NaOH.

(G and H) Composites of cellulose and CA/oPD-CPDs under natural light and UV light. (G) Composites with urea and LiOH. (H) The stiff and brighter part of the composites after removing extra urea and LiOH.

(I) Hand drawing obtained from CA/oPD-CPDs in HCl solution and FM in neutral solution.

See also Tables S2 and S3 and Figures S6–S9.

Besides different fluorescence peak positions, the fluorescence intensities also varied with different pH conditions. For FM, the highest fluorescence intensity was observed at the neutral condition, whereas for CA/oPD-CPDs, the fluorescence intensities were much higher at both acid and alkaline conditions (Figures 2D and 2E). This phenomenon is obviously different from reported CPDs (Bao et al., 2018; Kasprzyk et al., 2013) and makes it possible to apply CA/oPD-CPDs in cell death studies and other extreme pH situations. We believe it is because CA/oPD-CPDs aggregated at neutral condition, and the aggregated CA/oPD-CPDs further induced the self-quenching effect, which decreased the fluorescence intensity. This theory was further proved by the CA/oPD-CPDs and cellulose composites.

Due to the superior alkali resistance ability of the synthesized CA/oPD-CPDs, it is the best candidate for the fabrication of cellulose composites, which involves massive LiOH and urea (Wang et al., 2014). Figures 2G and 2H described the fluorescence of the composites remained bright even under extremely alkaline condition, and even increased after removing excess urea and LiOH (Figure 2H). At alkali condition, the enhanced dispersion of CA/oPD-CPDs in the composites retains the bright blue fluorescence. Although even the composite became neutral after removing urea and LiOH, the fluorescence of CA/oPD-CPDs was still witnessed owing to the restriction of the polymer network. This further proved that the aggregation of CA/oPD-CPDs at neutral condition was responsible for the quenching of fluorescence. Furthermore, the pH-dependent emission property of CA/oPD-CPDs and FM was additionally applied as fluorescence ink (Figure 2I).

To further investigate the fluorescence differences between FM and CA/oPD-CPDs, we tested the fluorescence lifetime of FM and CA/oPD-CPDs. As shown in Table S2, FM possessed a single lifetime, 9.42 ns at the neutral condition and 10.53 ns at alkaline condition, respectively. Although CA/oPD-CPDs showed two lifetimes, 2.5 ns related to the fluorescence from carbon core and 9.0 ns corresponding to fluorophores covalently anchored on the surface of carbon core. Noticeably, a new lifetime, 4.89 ns, appeared in the case of FM at acid condition, which could result from the aggregation of small molecules. At acid condition, the fluorescence spectra of FM presented slightly excitation-dependent behavior (Figure S6A), and the quantum yield of FM decreased to 43%, much lower than 83% at alkaline and neutral conditions (Table S3). Conclusively, we infer there are some aggregations of FM at acid condition. These aggregations at acid conditions change the surrounding environment and create a carbon-core similar situation, leading to the excitation-dependent behavior and the decreasing of PLQY. Analogously, this phenomenon was also found in other fluorescent organic molecules (Wang et al., 2015). As fluorescent materials, outstanding photostability is crucial for their further applications. After 8 h of continuous UV exposure, the fluorescence of the FM decreased to 32.58% (Figure S10). On contrast, 64.62% fluorescence of the CA/oPD-CPDs was preserved. The carbon core was supposed to partially protect the emission center, and even some fluorophores bonded covalently to the core was quenched by UV light (Zhai et al., 2012).

Besides UV exposure, cations could also influence the fluorescence intensity. We thus investigated the influence of different cations on CA/oPD-CPDs. To rule out the disturbance of cations to the pH of solutions, disodium hydrogen phosphate/citric acid buffer with pH 7.0 was chosen as the model solution. Herein, common metal ions in cell media, such as Na^+, K^+, Mg^{2+}, Ca^{2+}, Zn^{2+}, Al^{3+}, Ni^{2+}, Cu^{2+}, and Fe^{3+} at a concentration of 10^{-2}mol L^{-1} were added in CA/oPD-CPDs solutions (10 μg mL^{-1}; Figure S11). Similar to typical carbon nanodots, Fe^{3+} ion also had the obvious quenching effect on CA/oPD-CPDs (Zhu et al., 2013). For Ca^{2+}, Zn^{2+}, and Cu^{2+} ions, slight fluorescence variations can be attributed to the interactions between carboxylic groups and metal ions.

Selective Visualization of Lysosomes

As a tracking probe in biological events, cytotoxicity of CA/oPD-CPDs was first evaluated with MTT assay in human lung carcinoma (A549) cells. As shown in Figure 3A, when the concentration of CA/oPD-CPDs was 25 μg/mL, a sufficient concentration dosage for bioimaging, the cell viability of A549 was still 91.8%. When we further increased the incubation concentration to 50 μg/mL, the cell viability of A549 slightly decreased to 74.9%. These results indicated that the synthesized CA/oPD-CPDs were biocompatible and with extremely low toxicity within the concentration range for bioimaging, laying a solid foundation for the further application of CA/oPD-CPDs in biological fields.

We then examined whether the CA/oPD-CPDs can be adopted for lysosomes visualizing and tracking. The A549 cells were firstly incubated with CA/oPD-CPDs with a concentration of 25 μg/mL for 24 h. Then the cells were incubated with 100 nM LysoTracker Red DND99, a lysosome-targeting dye, to co-stain the lysosomes in cells. As shown in Figures 3B–3D, the blue fluorescence from CA/oPD-CPDs and the red fluorescence from LysoTracker Red overlapped with a high Pearson's correlation coefficient (a measure of the linear association of two variables, herein, fluorescence from CA/oPD-CPDs and those from LysoTracker Red) of 0.88, exceeding that of most lysosome-targeting nanoparticles. Lysosomes, acidic organelles with a pH around 4.8, play an important role in intracellular macromolecules degradation. Benefiting from the acidophilous property of CA/oPD-CPDs, we managed to visualize lysosomes in living cells passively without the involvement of additional lysosome-targeting molecular structure. Although CA/oPD-CPDs possess no selectivity in cells and spread over the whole cell, only the CA/oPD-CPDs in the lysosomes presented bright fluorescence due to the appropriate pH inside. Most CA/oPD-CPDs in the cytoplasm aggregated and presented extremely weak fluorescence. Thus, selective visualization of lysosomes was achieved with our pH-sensitive CA/oPD-CPDs. Because most pH-sensitive CPDs present weak fluorescence in acidic solution, the weak fluorescence from lysosomes will be covered by the strong fluorescence from cytoplasm and make it unable to visualize lysosomes without targeting groups. To the best of our knowledge, this is the first report of passive targeting CPDs applied in selective visualization of organelles. Moreover, compared with organic dyes with photostability issue, the CA/oPD-CPDs are able to preserve in living cells for 24 h without being degraded or causing cell death, which presents a possibility for long-time tracking of living cells.

Real-Time Intracellular pH Monitoring During Apoptosis

Besides selective visualization of lysosomes, CA/oPD-CPDs could also be applied for real-time cell pH monitoring during apoptosis. As discussed earlier, CA/oPD-CPDs possess no targeting groups and spread over

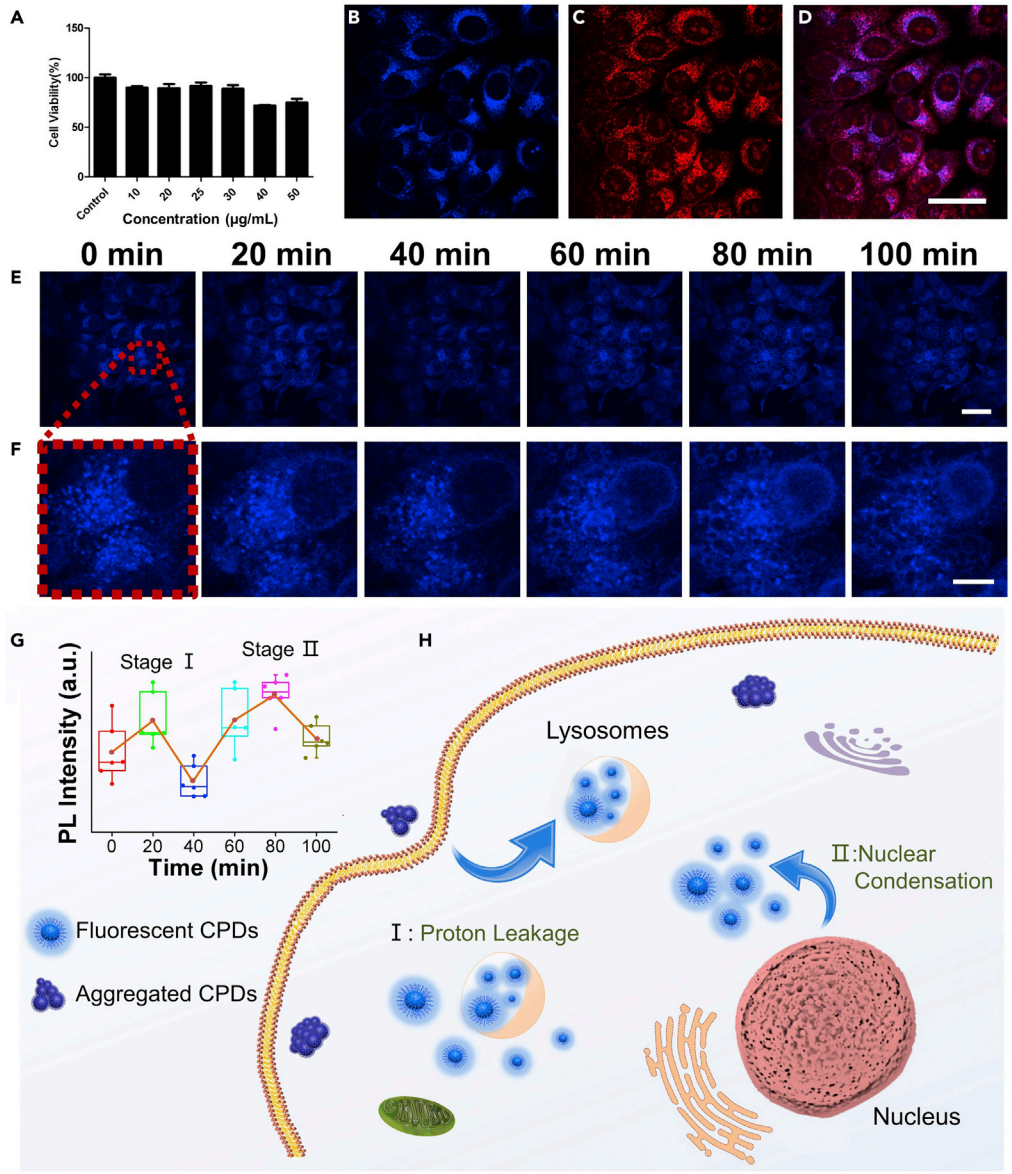

Figure 3. CA/oPD-CPDs for Lysosomes Imaging and Intracellular pH Monitoring

(A) Cytotoxicity assay of CA/oPD-CPDs on A549 cells (n = 3, Mean ± SD).

(B–D) Confocal fluorescence images of A549 cells co-stained with CA/oPD-CPDs and LysoTracker Red excited with (B) 405 nm and (C) 536 nm and (D) overlayed images of (B) and (C) (Scale bar: 40 μm).

(E and F) Real-time intracellular pH monitoring in living A549 cells during the apoptosis process. (E) Confocal fluorescence images of A549 cells incubated with CA/oPD-CPDs during apoptosis process on a large scale (Scale bar: 40 μm). (F) Magnified confocal fluorescence images of single A549 cell during the apoptosis (Scale bar: 10 μm).

(G) PL intensity variation of CA/oPD-CPDs in living cells at different apoptosis stage (n = 6, Mean ± SD).

(H) The intracellular trafficking and transformation of CA/oPD-CPDs during apoptosis.

See also Figures S12 and S13.

the cytoplasm. CA/oPD-CPDs possess extremely weak fluorescence in the healthy living cells owing to the neutral physiological pH value. Only the well-dispersed CA/oPD-CPDs in the lysosomes present bright blue emission. Thus, the aggregated CA/oPD-CPDs in living cells could be used to monitor the intracellular pH change during apoptosis. After incubation for 24 h with CA/oPD-CPDs, a strong blue fluorescence from CA/oPD-CPDs in the lysosomes was observed as shown in Figure 3E. We then used dexamethasone (a chemotherapeutic agent) to induce apoptosis of living cells. Without the addition of dexamethasone, the fluorescence

intensity from the control group (CA/oPD-CPDs only) continuously decreased due to photobleaching under UV light (Figure S12). After four times of exposure, the original fluorescence intensity decreased a lot (Figure S13). For the experiment group (CA/oPD-CPDs with the addition of dexamethasone), the fluorescence intensity from the whole cell involves two stages of fluorescence increasing, as shown in Figure 3E. After 20-min treatment by dexamethasone, the first stage originated from proton leakage from lysosomes. The fluorescence intensity slightly increased (Figure 3G). In the magnified image (Figure 3F) the contour of lysosomes became fuzzy at the first stage. Due to proton leakage, the pH inside the lysosomes increased and the fluorescence of CA/oPD-CPDs in the lysosomes was suppressed. However, the leaked proton illuminated the CA/oPD-CPDs in the cytoplasm around the lysosomes. Thus, the contour of lysosomes became unclear and the fluorescence from the whole cell slightly increased even under the influence of photobleaching. After 40 min, the fluorescence intensity decreased due to photobleaching. During the apoptosis process, proton leakage takes place firstly, following by the second stage, nuclear condensation. The nuclear acid and other organic acids were leaked through the nuclear envelope, further decreasing the pH in the cytoplasm. Thus, the aggregated CA/oPD-CPDs in the cytoplasm were illuminated with the acidic materials around nuclear envelope after the addition of dexamethasone for 60 min. As shown in Figure 3G, the fluorescence intensity further increased for whole cells indicating the decrease of intracellular pH. Moreover, the nuclear envelop contour was also illuminated and getting condensed during the apoptosis process. For other pH-sensitive CPDs, the fluorescence intensity always decreases during apoptosis, similar to the tendency caused by photobleaching, which makes it unapparent to monitor the intracellular pH variation without a control group. Different from other reports, the fluorescence intensity of the synthesized CA/oPD-CPDs increased obviously during apoptosis even with the influence of photobleaching. Benefitting from their aggregation-dissociation induced PL behavior, CA/oPD-CPDs achieved persistently recording of intracellular pH during apoptosis even with partial photobleaching issue.

Laser-Induced Fluorescence Enhancement for Living Cells

Besides selective visualization of lysosomes and intracellular pH monitoring, another fascinating feature of our CA/oPD-CPDs is the laser-induced fluorescence enhancement. Fluorescence loss under laser irradiation is hindering the development of most bioimaging agents, particularly under the laser confocal microscopy. LysoTracker Red is a representative commercial lysosomal dye, whose fluorescence intensity quickly decreased within 3-min exposure (Figures 4A and 4C). In contrast, the synthesized CA/oPD-CPDs presented a continuous fluorescence increase under laser irradiation in living cells within 2 h (Figures 4B and 4D, A549 cells (human non-small cell lung cancer cell lines, cancer cells) were cultured with CA/oPD-CPDs in advance for 24 h to promote efficient endocytosis). To understand this phenomenon, several control experiments were conducted. For CA/oPD-CPDs aqueous solution, no fluorescence increase was observed with blue-light exposure (Figure 4E). When living A549 cells with CA/oPD-CPDs were exposed under blue light *in vitro* with different times, the fluorescence intensity increased with longer exposure time (Figure 4F). To verify the universality of this fluorescence enhancement, L929 cells (mouse-derived fibroblast cells, normal cells) were also applied. As shown in Figure S14, L929 cells also presented a continuous fluorescence enhancement under laser confocal microscopy. The fluorescence enhancement was also observed with fluorescence spectroscopy (Figure 4G). Because L929 cells are normal cells, they are more vulnerable than A549 cells. Under the same blue light exposure, the cytoplasm of L929 cells turned acid faster than A549 cells, leading to a higher fluorescence enhancement (insets of Figures 4F and 4G) under the same exposure time. Thus, we supposed that the CA/oPD-CPDs with blue light could induce slowly death of living cells by reactive oxygen species. Photodynamic therapy (PDT) can cause irreversible damage to cells through reactive oxygen species (ROS) that are generated by photosensitizers (PS). The death of cells will inevitably cause the acidification in cytoplasm (Gottlieb et al., 1995, 1996; Zanke et al., 1998). Among all the applications of CPDs, unmodified CPDs as photosensitizers applied in photodynamic therapy are still uncommon (Du et al., 2019; Lu et al., 2019; Zhang et al., 2018a). Herein, the generated ROS from CA/oPD-CPDs under blue light caused cell damage, leading to the acidification of cytoplasm, and further increased the fluorescence of CA/oPD-CPDs in cells. To prove this theory, the cytotoxicity of CA/oPD-CPDs with blue light was tested. When the concentration of CA/oPD-CPDs was 25 μg/mL, the cell viability of A549 was 21% with 2-h 15 W blue light exposure but 91% without blue light exposure (Figure 4H). Then, the DCFH-DA fluorescent probe was applied to confirm the existence of ROS. Fluorescence intensity from DCFH-DA with CA/oPD-CPDs under blue light increased dramatically compared with the control group (Figure S15), which confirmed that CA/oPD-CPDs could generate ROS under blue light exposure. To further confirm this assumption, the fluorescence behavior of fixed cells (dead cells) under laser confocal microscopy was tested. As shown in Figure S16, the fluorescence intensity from fixed A549 cells expectedly decreased with longer laser exposure time. Based on these experiments, we believe that the acidification of living cells under laser exposure is responsible for the

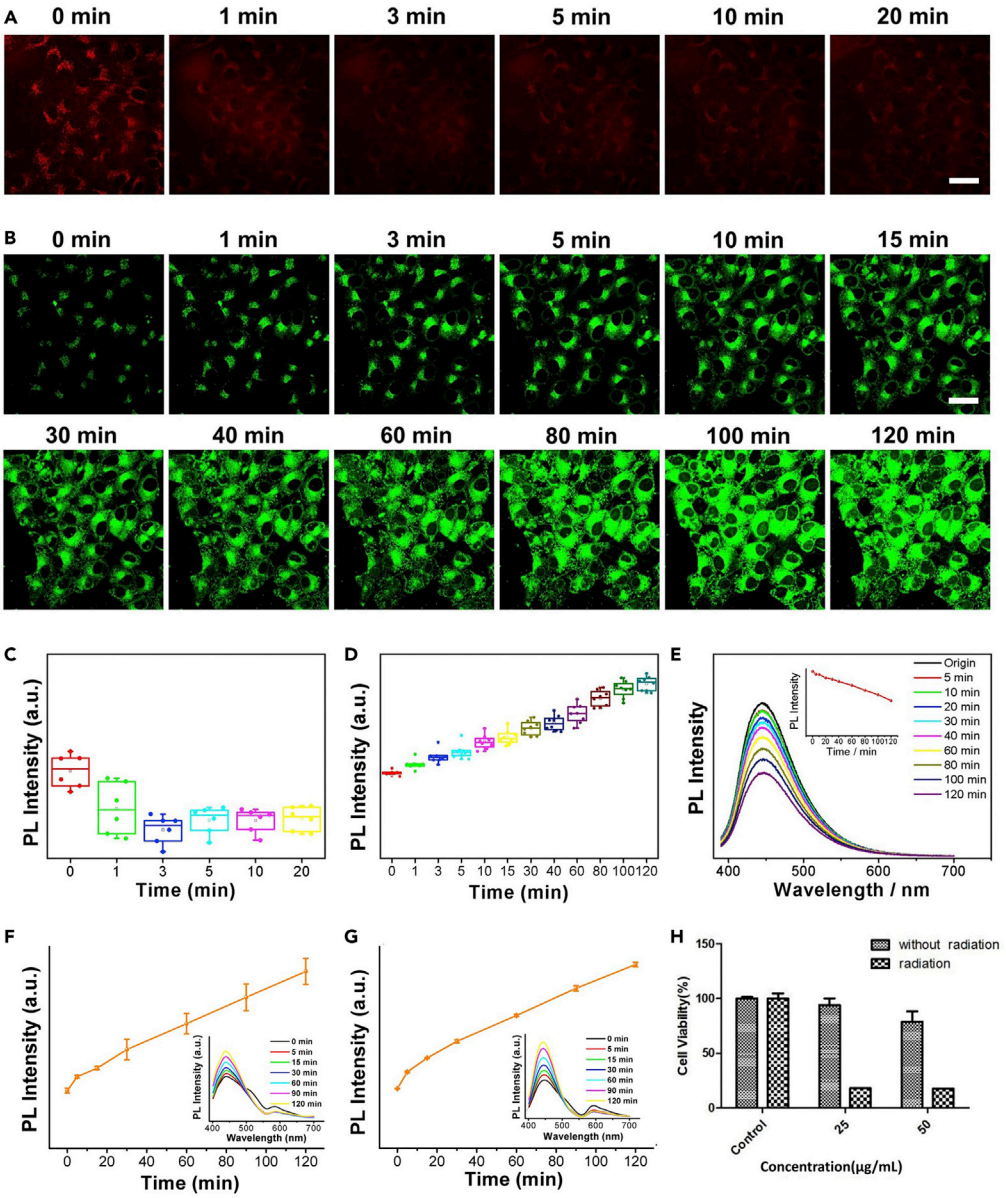

Figure 4. Laser-Induced Fluorescence Enhancement of CA/oPD-CPDs in Living Cells

(A and C) A549 cells stained with Lyso-Tracker Red continuously exposed for different periods under 536 nm laser irradiation. (A) confocal fluorescence images and (C) corresponding PL intensity variation (Scale bar: 40 μm; n=6, Mean ± SD).

(B and D) A549 cells stained with CA/oPD-CPDs continuously exposed for different periods under 488 nm laser irradiation. (B) confocal fluorescence images and (D) corresponding PL intensity variation (Scale bar: 40 μm; n=8, Mean ± SD).

(E) PL spectra and intensity variation of CA/oPD-CPDs aqueous solution for different exposure periods under 488 nm in neutral aqueous solution.

(F and G) PL intensity variation and spectra of living (F) A549 cells (n = 3, Mean ± SD) and (G) L929 cells suspension (n = 3, Mean ± SD) incubated with CA/oPD-CPDs for different exposure periods under 488 nm (tested with fluorescence spectroscopy).

(H) Cytotoxicity assay on A549 cells of CA/oPD-CPDs with and without 2-h 15 W blue light exposure (n = 3, Mean ± SD). See also Figures S14–S16.

fluorescence enhancement of CA/oPD-CPDs. Additionally, the synthesized CA/oPD-CPDs also present a potential utilization as photodynamic agents for cancer therapy.

Conclusion

In summary, we synthesized a kind of CA/oPD-CPDs with unconventional pH sensitivity from citric acid and o-phenylenediamine via a hydrothermal process. We not only confirmed the co-existence of fluorescent molecules and CA/oPD-CPDs but also separated them with a simple method and fully investigated their differences. The synthesized CA/oPD-CPDs presented bright fluorescence at acidic and alkaline conditions but weak fluorescence in the neutral environment. Benefitting from this property, we achieved passive lysosomes visualization. Further more, the aggregated dormient CA/oPD-CPDs in the cytoplasm were able to monitor real-time intracellular pH variation during apoptosis of living cells including the proton leakage and cell nuclear condensation. Moreover, as a bioimaging agent, the CA/oPD-CPDs presented a continuous fluorescence enhancement under laser irradiation, which laid a solid foundation for single-cell long-term tracking. Developing unconventional pH-responsive CPDs that are non-toxic and can be preserved in living cells within a long period is highly meaningful and provides useful modality on the study of cell fate, cell viability, and the efficiency of anti-cancer drugs.

Limitations of the Study

Although the synthesized CA/oPD-CPDs are sensitive to pH and could track the intracellular pH variation, the UV-induced photobleaching is still hindering the quantification of specific intracellular pH.

METHODS

All methods can be found in the accompanying Transparent Methods supplemental file.

SUPPLEMENTAL INFORMATION

Supplemental Information can be found online at https://doi.org/10.1016/j.isci.2020.100982.

ACKNOWLEDGMENTS

This work was financially supported by the National Science Foundation of China (NSFC) under Grant Nos. 51433003, 21774041 and JLU Science and Technology Innovative Research Team 2017TD-06.

AUTHOR CONTRIBUTIONS

B.Y. and S.Z. conceived and supervised the research. X.Z. performed all the experiments. J.L.,D.L.,M.Y., and W.W. helped to perform biology experiments. X.Z. wrote the manuscript.

DECLARATION OF INTERESTS

The authors declare no competing interests.

Received: December 13, 2019
Revised: February 23, 2020
Accepted: March 7, 2020
Published: April 24, 2020

REFERENCES

Appelqvist, H., Waster, P., Kagedal, K., and Ollinger, K. (2013). The lysosome: from waste bag to potential therapeutic target. J. Mol. Cell Biol. *5*, 214–226.

Baker, S.N., and Baker, G.A. (2010). Luminescent carbon nanodots: emergent nanolights. Angew. Chem. Int. Ed. *49*, 6726–6744.

Bao, Y.W., Hua, X.W., Li, Y.H., Jia, H.R., and Wu, F.G. (2018). Hyperthemia-promoted cytosolic and nuclear delivery of copper/carbon quantum dot-crosslinkednanosheets: multimodal imaging-guided photothermal cancer therapy. ACS Appl. Mater. Interfaces *10*, 1544–1555.

Cai, Y., Gui, C., Samedov, K., Su, H., Gu, X., Li, S., Luo, W., Sung, H.H.Y., Lam, J.W.Y., Kwok, R.T.K., et al. (2017). An acidic pH independent piperazine-TPEAIEgen as a unique bioprobe for lysosome tracing. Chem. Sci. *8*, 7593–7603.

Cao, L., Meziani, M.J., Sahu, S., and Sun, Y.P. (2013). Photoluminescence properties of graphene versus other carbon nanomaterials. Acc. Chem. Res. *46*, 171–180.

Cayuela, A., Soriano, M.L., Carrillo-Carrion, C., and Valcarcel, M. (2016). Semiconductor and carbon-based fluorescent nanodots: the need for consistency. Chem. Commun. *52*, 1311–1326.

Chen, Z., Zeng, Q., Liu, F., Jin, G., Du, X., Du, J., Zhang, H., and Yang, B. (2015). Efficient inorganic solar cells from aqueous nanocrystals: the impact of composition on carrier dynamics. RSC Adv. *5*, 74263–74269.

Dong, Y., Cai, J., You, X., and Chi, Y. (2015). Sensing applications of luminescent carbon based dots. Analyst *140*, 7468–7486.

Du, J., Xu, N., Fan, J., Sun, W., and Peng, X. (2019). Carbon dots for in Vivo bioimaging and theranostics. Small *15*, e1805087.

E, S., Mao, Q.X., Yuan, X.L., Kong, X.L., Chen, X.W., and Wang, J.H. (2018). Targeted imaging of the lysosome and endoplasmic reticulum and their pH monitoring with surface regulated carbon dots. Nanoscale *10*, 12788–12796.

Feng, T., Zeng, Q., Lu, S., Yan, X., Liu, J., Tao, S., Yang, M., and Yang, B. (2017). Color-tunable carbon dots possessing solid-state emission for full-color light-emitting diodes applications. ACS Photonics *5*, 502–510.

Gao, G., Jiang, Y.W., Yang, J., and Wu, F.G. (2017). Mitochondria-targetable carbon quantum dots for differentiating cancerous cells from normal cells. Nanoscale *9*, 18368–18378.

Gottlieb, R., Giesing, H., Zhu, J., Engler, R., and Babior, B. (1995). Cell acidification in apoptosis: granulocyte colony-stimulating factor delays programed cell death in neutrophils by up-regulating the vacuolar H^+-ATPase. Proc. Natl. Acad. Sci. U S A *92*, 5965–5968.

Gottlieb, R., Nordberg, J., Skowronski, E., and Babior, B. (1996). Apoptosis induced in Jurkat cells by several agents is preceded by intracellular acidification. Proc. Natl. Acad. Sci. U S A *93*, 654–658.

Gupta, V., Chaudhary, N., Srivastava, R., Sharma, G.D., Bhardwaj, R., and Chand, S. (2011). Luminscentgraphene quantum dots for organic photovoltaic devices. J. Am. Chem. Soc. *133*, 9960–9963.

Hu, Y., Yang, J., Tian, J., Jia, L., and Yu, J.-S. (2014). Waste frying oil as a precursor for one-step synthesis of sulfur-doped carbon dots with pH-sensitive photoluminescence. Carbon *77*, 775–782.

Hua, X.W., Bao, Y.W., Chen, Z., and Wu, F.G. (2017). Carbon quantum dots with intrinsic mitochondrial targeting ability for mitochondria-based theranostics. Nanoscale *9*, 10948–10960.

Hua, X.W., Bao, Y.W., and Wu, F.G. (2018). Fluorescent carbon quantum dots with intrinsic nucleolus-targeting capability for nucleolus imaging and enhanced cytosolic and nuclear drug delivery. ACS Appl. Mater. Interfaces *10*, 10664–10677.

Hua, X.W., Bao, Y.W., Zeng, J., and Wu, F.G. (2019). Nucleolus-targeted red emissive carbon dots with polarity-sensitive and excitation-independent fluorescence emission: high-resolution cell imaging and in Vivo tracking. ACS Appl. Mater. Interfaces *11*, 32647–32658.

Jiang, J., He, Y., Li, S., and Cui, H. (2012). Amino acids as the source for producing carbon nanodots: microwave assisted one-step synthesis, intrinsic photoluminescence property and intense chemiluminescence enhancement. Chem. Commun. *48*, 9634–9636.

Jin, H., Huang, H., He, Y., Feng, X., Wang, S., Dai, L., and Wang, J. (2015). Graphene quantum dots supported by graphenenanoribbons with ultrahigh electrocatalytic performance for oxygen reduction. J. Am. Chem. Soc. *137*, 7588–7591.

Kasprzyk, W., Bednarz, S., and Bogdal, D. (2013). Luminescence phenomena of biodegradable photoluminescentpoly(diol citrates). Chem. Commun. *49*, 6445–6447.

Kasprzyk, W., Bednarz, S., Żmudzki, P., Galica, M., and Bogdał, D. (2015). Novel efficient fluorophores synthesized from citric acid. RSC Adv. *5*, 34795–34799.

Khan, S., Verma, N.C., Chethana, and Nandi, C.K. (2018). Carbon dots for single-molecule imaging of the nucleolus. ACS Appl. Nano Mater. *1*, 483–487.

Kong, B., Zhu, A., Ding, C., Zhao, X., Li, B., and Tian, Y. (2012). Carbon dot-based inorganic-organic nanosystem for two-photon imaging and biosensing of pH variation in living cells and tissues. Adv. Mater. *24*, 5844–5848.

Krysmann, M.J., Kelarakis, A., Dallas, P., and Giannelis, E.P. (2012). Formation mechanism of carbogenic nanoparticles with dual photoluminescence emission. J. Am. Chem. Soc. *134*, 747–750.

Li, H., He, X., Kang, Z., Huang, H., Liu, Y., Liu, J., Lian, S., Tsang, C.H., Yang, X., and Lee, S.T. (2010). Water-soluble fluorescent carbon quantum dots and photocatalyst design. Angew. Chem. Int. Ed. *49*, 4430–4434.

Li, H., Kang, Z., Liu, Y., and Lee, S.-T. (2012). Carbon nanodots: synthesis, properties and applications. J. Mater. Chem. *22*, 24230–24253.

Li, R.S., Gao, P.F., Zhang, H.Z., Zheng, L.L., Li, C.M., Wang, J., Li, Y.F., Liu, F., Li, N., and Huang, C.Z. (2017). Chiral nanoprobes for targeting and long-term imaging of the Golgi apparatus. Chem. Sci. *8*, 6829–6835.

Liu, C., Zhang, P., Zhai, X., Tian, F., Li, W., Yang, J., Liu, Y., Wang, H., Wang, W., and Liu, W. (2012). Nano-carrier for gene delivery and bioimaging based on carbon dots with PEI-passivation enhanced fluorescence. Biomaterials *33*, 3604–3613.

Liu, J.J., Zhang, X.L., Cong, Z.X., Chen, Z.T., Yang, H.H., and Chen, G.N. (2013). Glutathione-functionalized graphene quantum dots as selective fluorescent probes for phosphate-containing metabolites. Nanoscale *5*, 1810–1815.

Lu, S., Zhao, X., Zhu, S., Song, Y., and Yang, B. (2014). Novel cookie-with-chocolate carbon dots displaying extremely acidophilic high luminescence. Nanoscale *6*, 13939–13944.

Lu, W., Jiao, Y., Gao, Y., Qiao, J., Mozneb, M., Shuang, S., Dong, C., and Li, C.Z. (2018). Bright yellow fluorescent carbon dots as a multifunctional sensing platform for the label-free detection of fluoroquinolones and histidine. ACS Appl. Mater. Interfaces *10*, 42915–42924.

Lu, Z., Liu, S., Le, Y., Qin, Z., He, M., Xu, F., Zhu, Y., Zhao, J., Mao, C., and Zheng, L. (2019). An injectable collagen-genipin-carbon dot hydrogel combined with photodynamic therapy to enhance chondrogenesis. Biomaterials *218*, 119190.

Nilsson, C., Kågedal, K., Johansson, U., and Öllinger, K. (2004). Analysis of cytosolic and lysosomal pH in apoptotic cells by flow cytometry. Methods Cell Sci. *25*, 185–194.

Qu, S., Wang, X., Lu, Q., Liu, X., and Wang, L. (2012). A biocompatible fluorescent ink based on water-soluble luminescent carbon nanodots. Angew. Chem. Int. Ed. *51*, 12215–12218.

Qu, D., Zheng, M., Zhang, L., Zhao, H., Xie, Z., Jing, X., Haddad, R.E., Fan, H., and Sun, Z. (2014a). Formation mechanism and optimization of highly luminescent N-doped graphene quantum dots. Sci. Rep. *4*, 5294.

Qu, S., Liu, X., Guo, X., Chu, M., Zhang, L., and Shen, D. (2014b). Amplified spontaneous green emission and lasing emission from carbon nanoparticles. Adv. Funct. Mater. *24*, 2689–2695.

Saftig, P., and Klumperman, J. (2009). Lysosome biogenesis and lysosomal membrane proteins: trafficking meets function. Nat. Rev. Mol. Cell Biol. *10*, 623–635.

Song, Y., Zhu, S., Zhang, S., Fu, Y., Wang, L., Zhao, X., and Yang, B. (2015). Investigation from chemical structure to photoluminescent mechanism: a type of carbon dots from the pyrolysis of citric acid and an amine. J. Mater. Chem. C *3*, 5976–5984.

Wang, Z., Fan, X., He, M., Chen, Z., Wang, Y., Ye, Q., Zhang, H., and Zhang, L. (2014). Construction of cellulose-phosphor hybrid hydrogels and their application for bioimaging. J. Mater. Chem. B *2*, 7559–7566.

Wang, Y., Zhang, I., Yu, B., Fang, X., Su, X., Zhang, Y.-M., Zhang, T., Yang, B., Li, M., and Zhang, S.X.-A. (2015). Full-color tunable mechanofluorochromism and excitation-dependent emissions of sngle-arm extended tetraphenylethylenes. J. Mater. Chem. C *3*, 12328–12334.

Wang, Q., Yang, H., Zhang, Q., Ge, H., Zhang, S., Wang, Z., and Ji, X. (2019). Strong acid-assisted preparation of green-emissive carbon dots for fluorometric imaging of pH variation in living cells. Microchim. Acta *186*, 468.

Wu, Z.L., Gao, M.X., Wang, T.T., Wan, X.Y., Zheng, L.L., and Huang, C.Z. (2014). A general quantitative pH sensor developed with dicyandiamide N-doped high quantum yield graphene quantum dots. Nanoscale *6*, 3868–3874.

Wu, L., Li, X., Ling, Y., Huang, C., and Jia, N. (2017). Morpholine derivative-functionalized carbon dots-based fluorescent probe for highly selective lysosomal imaging in living cells. ACS Appl. Mater. Interfaces *9*, 28222–28232.

Xia, C., Zhu, S., Feng, T., Yang, M., and Yang, B. (2019). Evolution and synthesis of carbon dots: from carbon dots to carbonized polymer dots. Adv. Sci. *6*, 1901316.

Yang, Z.C., Wang, M., Yong, A.M., Wong, S.Y., Zhang, X.H., Tan, H., Chang, A.Y., Li, X., and Wang, J. (2011). Intrinsically fluorescent carbon dots with tunable emission derived from hydrothermal treatment of glucose in the presence of monopotassium phosphate. Chem. Commun. *47*, 11615–11617.

Yang, K., Feng, L., Shi, X., and Liu, Z. (2013). Nano-graphene in biomedicine: theranostic applications. Chem. Soc. Rev. *42*, 530–547.

Yuan, M., Guo, Y., Wei, J., Li, J., Long, T., and Liu, Z. (2017). Optically active blue-emitting carbon dots to specifically target the Golgi apparatus. RSCAdv. *7*, 49931–49936.

Zanke, B., Lee, C., Arab, S., and Tannock, I. (1998). Death of tumor cells after intracellular acidification is dependent on stress-activated protein kinases (SAPK/JNK) pathway activation

and cannot be inhibited by bcl-2 expression or interleukin 1β-converting enzyme inhibition. Cancer Res. *58*, 2801–2808.

Zhai, X., Zhang, P., Liu, C., Bai, T., Li, W., Dai, L., and Liu, W. (2012). Highly luminescent carbon nanodots by microwave-assisted pyrolysis. Chem. Commun. *48*, 7955–7957.

Zhang, Z., Zhang, J., Chen, N., and Qu, L. (2012). Graphene quantum dots: an emerging material for energy-related applications and beyond. Energy Environ. Sci. *5*, 8869–8890.

Zhang, L., Zhang, Z.Y., Liang, R.P., Li, Y.H., and Qiu, J.D. (2014). Boron-doped graphene quantum dots for selective glucose sensing based on the "abnormal" aggregation-induced photoluminescence enhancement. Anal. Chem. *86*, 4423–4430.

Zhang, L., Lin, Z., Yu, Y.-X., Jiang, B.-P., and Shen, X.-C. (2018a). Multifunctional hyaluronic acid-derived carbon dots for self-targeted imaging-guided photodynamic therapy. J. Mater. Chem. B *6*, 6534–6543.

Zhang, Q.Q., Yang, T., Li, R.S., Zou, H.Y., Li, Y.F., Guo, J., Liu, X.D., and Huang, C.Z. (2018b). A functional preservation strategy for the production of highly photoluminescent emerald carbon dots for lysosome targeting and lysosomal pH imaging. Nanoscale *10*, 14705–14711.

Zhao, X., Zhu, S., Song, Y., Zhang, J., and Yang, B. (2015). Thermal responsive fluorescent nanocomposites based on carbon dots. RSC Adv. *5*, 15187–15193.

Zhao, X., Tang, Q., Zhu, S., Bu, W., Yang, M., Liu, X., Meng, Y., Yu, W., Sun, H., and Yang, B. (2019). Controllable acidophilic dual-emission fluorescent carbonized polymer dots for selective imaging of bacteria. Nanoscale *11*, 9526–9532.

Zheng, X.T., Ananthanarayanan, A., Luo, K.Q., and Chen, P. (2015). Glowing graphene quantum dots and carbon dots: properties, syntheses, and biological applications. Small *11*, 1620–1636.

Zhu, S., Meng, Q., Wang, L., Zhang, J., Song, Y., Jin, H., Zhang, K., Sun, H., Wang, H., and Yang, B. (2013). Highly photoluminescent carbon dots for multicolor patterning, sensors, and bioimaging. Angew. Chem. Int. Ed. *52*, 3953–3957.

Zhu, S., Song, Y., Zhao, X., Shao, J., Zhang, J., and Yang, B. (2015). The photoluminescence mechanism in carbon dots (graphene quantum dots, carbon nanodots, and polymer dots): current state and future perspective. Nano Res. *8*, 355–381.

Zhu, S., Zhao, X., Song, Y., Lu, S., and Yang, B. (2016). Beyond bottom-up carbon nanodots: citric-acid derived organic molecules. Nano Today *11*, 128–132.

iScience, Volume *23*

Supplemental Information

Self-Enhanced Carbonized Polymer Dots for Selective Visualization of Lysosomes and Real-Time Apoptosis Monitoring

Xiaohuan Zhao, Jing Li, Dongning Liu, Mingxi Yang, Wenjing Wang, Shoujun Zhu, and Bai Yang

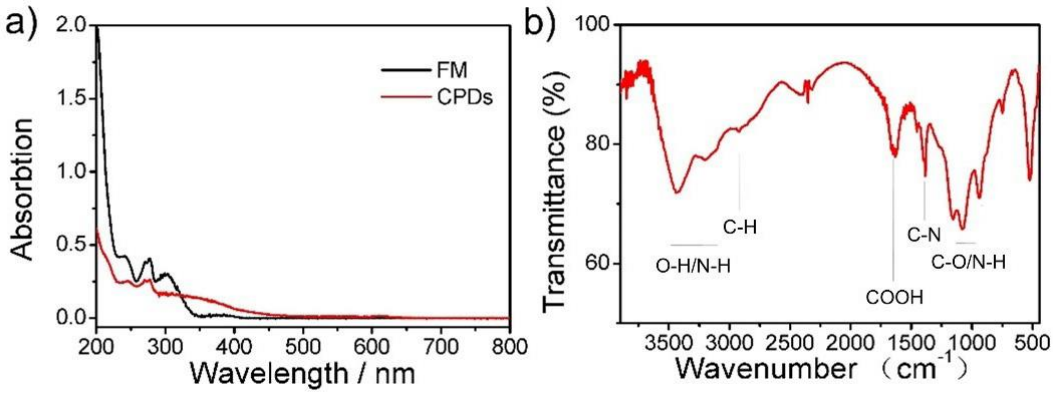

Figure S1. a) UV-vis absorption of FM and CA/oPD-CPDs in neutral aqueous solution. b) FTIR spectrum of CA/oPD-CPDs powder. Related to Figure 1.

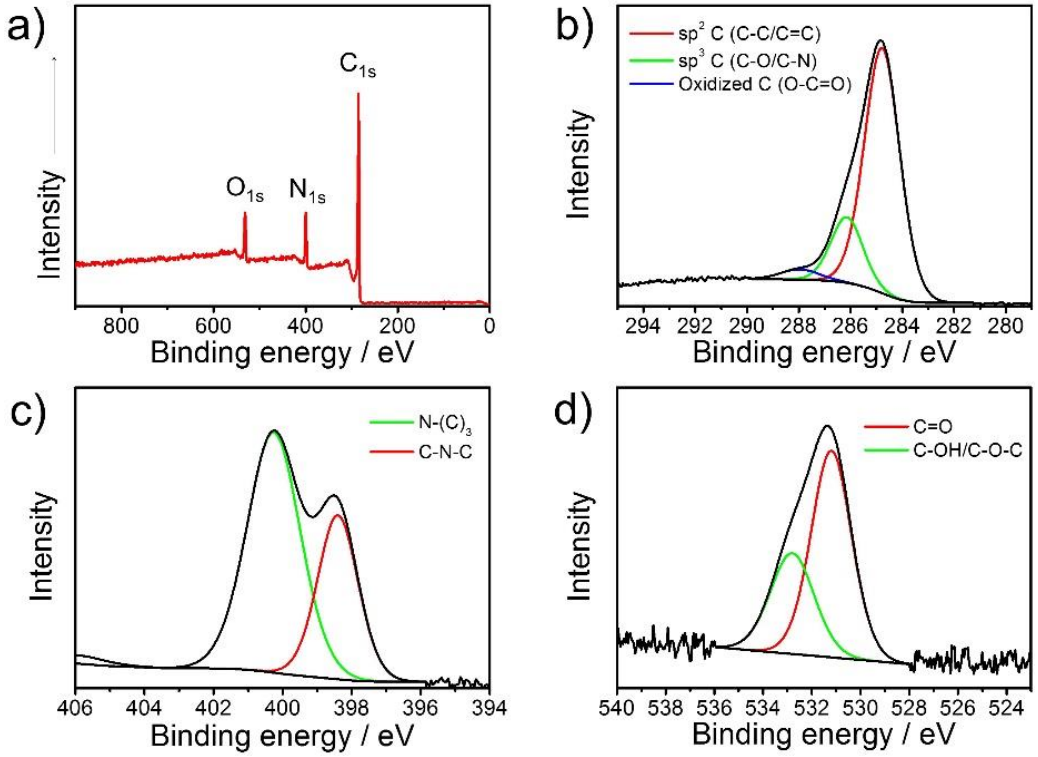

Figure S2. XPS spectra of CA/oPD-CPDs, which were tested with CA/oPD-CPDs powder on glass. Related to Figure 1.

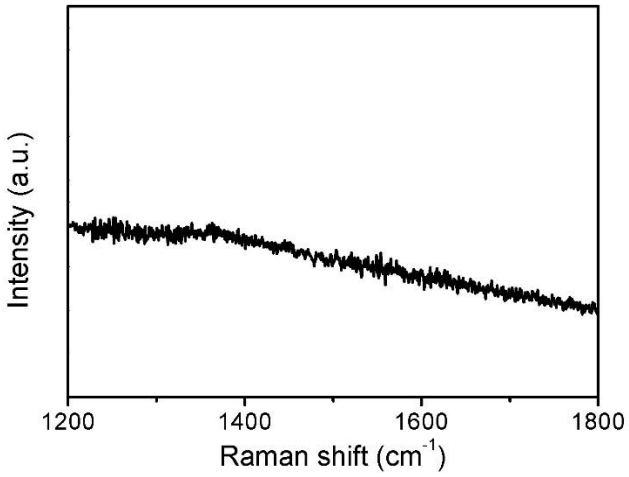

Figure S3. The Raman spectrum of CA/oPD-CPDs (tested with CA/oPD-CPDs powder on glass). Related to Figure 1.

Table S1. Elemental analysis of CA/oPD-CPDs which was tested with CA/oPD-CPDs powder. Related to Figure 1.

Element	C(%)	N(%)	H(%)	O (Calculated)(%)
CA/oPD-CPDs	66.97%	15.17%	4.57%	13.29%

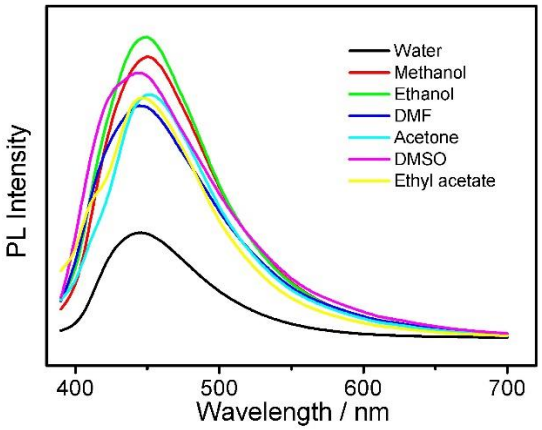

Figure S4. Fluorescence spectra of CA/oPD-CPDs in neutral pH aqueous solution and other different organic solvents. Related to Figure 1.

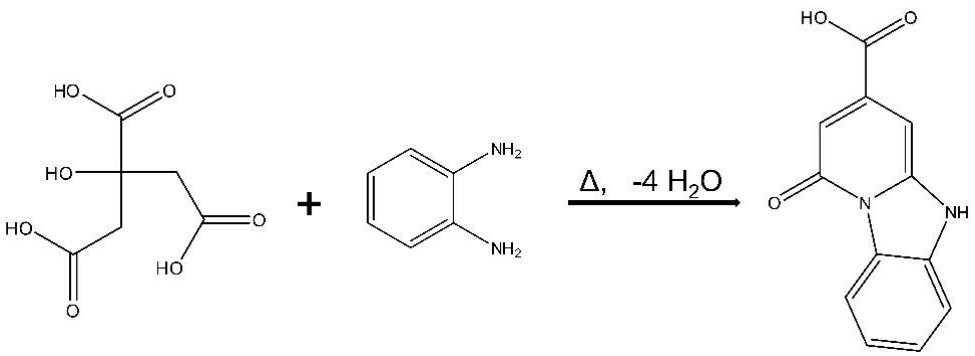

Figure S5. Scheme of the primary reaction of citric acid and o-phenylenediamine. Related to Figure 1.

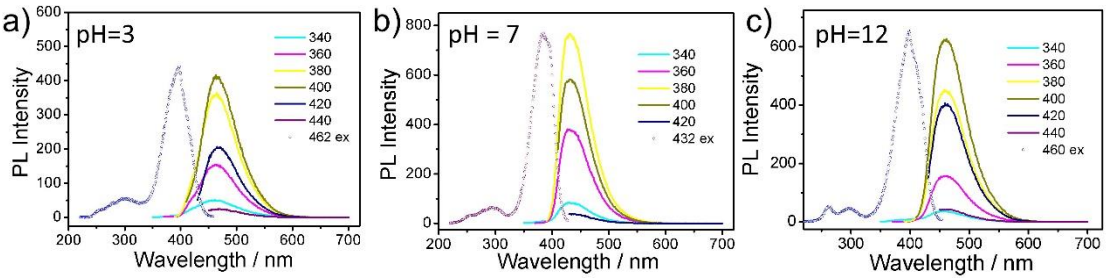

Figure S6. PL spectra of FM with different excitation wavelengths in a) pH 3, b) pH 7, and c) pH 12 aqueous solutions with either HCl or NaOH. Related to Figure 2.

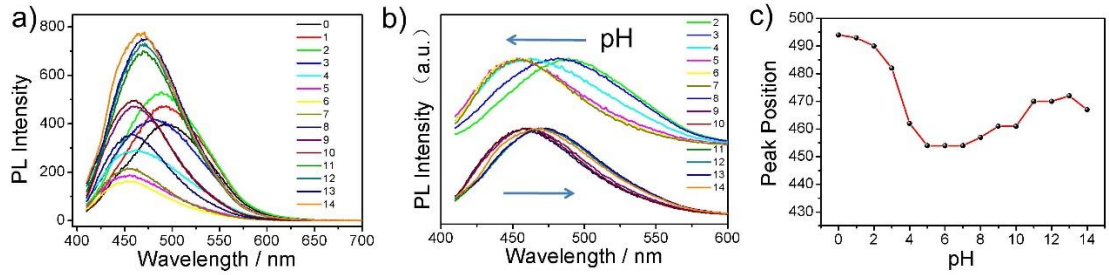

Figure S7. a) The PL spectra of CA/oPD-CPDs excited with 380 nm at different pH conditions and b) the normalized PL spectra. c) PL peak positions of CA/oPD-CPDs at different pH conditions. The PL spectra were tested in different pH aqueous solutions with HCl, NaOH or citric acid/disodium hydrogen phosphate buffers. Related to Figure 2.

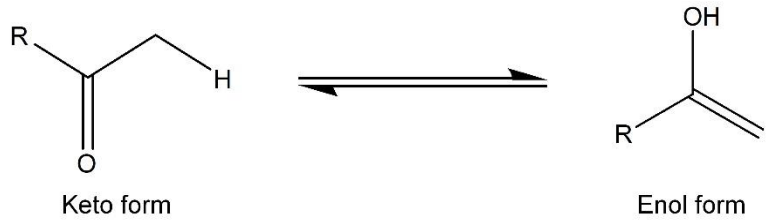

Figure S8. Scheme of the Keto-Enol Tautomerism. Related to Figure 2.

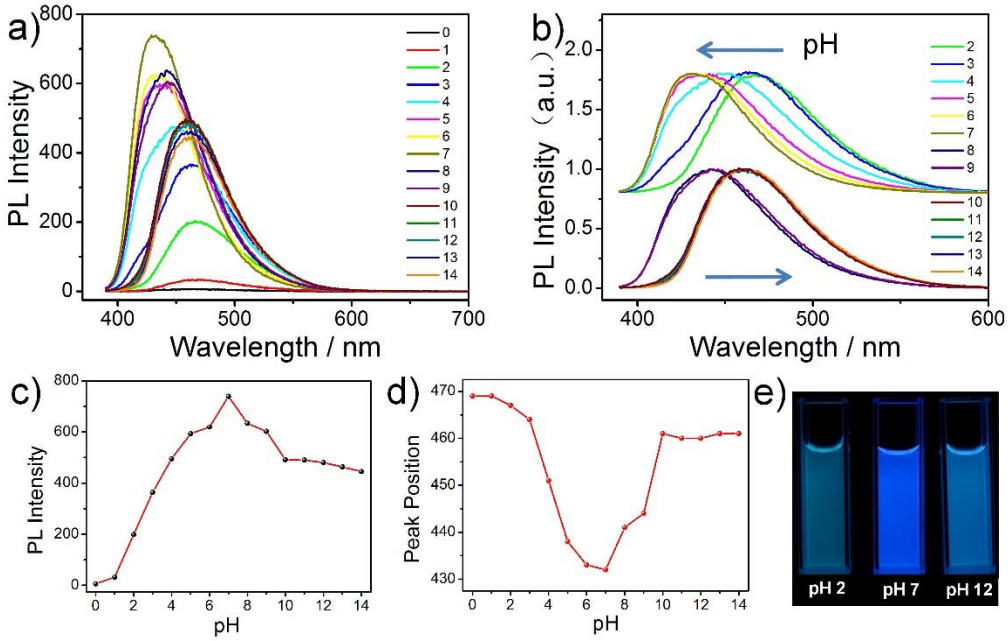

Figure S9. a) The PL spectra of FM at different pH conditions. b) Normalized PL spectra of FM. c) PL intensities and d) PL peak positions of FM at different pH conditions. e) Digital photos of FM solutions at pH 2, pH 7, and pH 12. The PL spectra were tested in different pH aqueous solutions with HCl, NaOH or citric acid/disodium hydrogen phosphate buffers. Related to Figure 2.

Table S2. The Fluorescence lifetime of FM and CA/oPD-CPDs (tested in different pH aqueous solutions with either HCl or NaOH). Related to Figure 2.

	pH 2		**pH 7**		**pH 12**	
FM	4.89 ns	10.64 ns	9.42 ns		10.53 ns	
	12.36%	87.64%	100%		100%	
	9.93 ns		9.42 ns		10.53 ns	
CA/oPD-CPDs	2.39 ns	8.64 ns	3.13 ns	9.14 ns	2.53 ns	9.31 ns
	23.66%	76.34%	20.57%	79.43%	26.87%	73.13 %
	7.16 ns		7.90 ns		7.49 ns	

Table S3. PLQY of FM and CA/oPD-CPDs at pH 2, pH 7, pH 12. Related to Figure 2.

pH	2	7	12
FM	43%	83%	83%
CA/oPD-CPDs	19.9%	5.79%	20.16%

Note: CA/oPD-CPDs and Fluorescent Molecule were dispersed as very dilute solutions in pure water (pH 7), water with HCl (pH 2), and water with NaOH (pH 12), respectively. The absolute quantum yields were tested with an excitation wavelength of 380 nm.

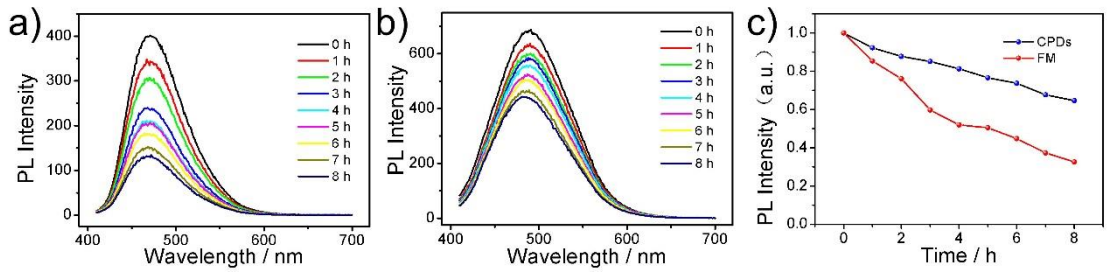

Figure S10. PL spectra of a) FM and b) CA/oPD-CPDs at pH 2 aqueous solutions with HCl under continuous UV exposure. c) PL intensity decreasing tendency of FM and CA/oPD-CPDs. Related to Figure 2.

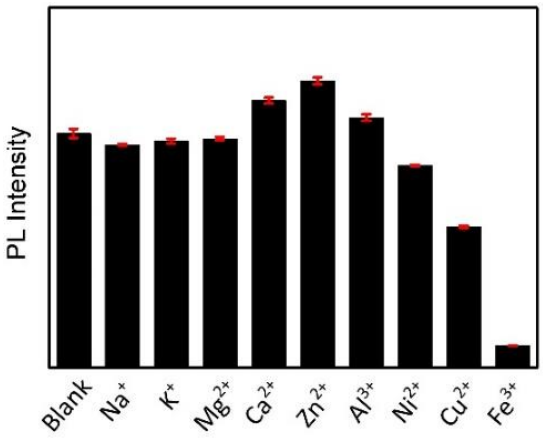

Figure S11. Comparison of fluorescence intensities of CA/oPD-CPDs (10 μg mL^{-1}) after the addition of different metal ions (10^{-2} mol L^{-1}**)**. (Due to the pH sensitivity of CA/oPD-CPDs, the PL intensities were tested in pH 7 citric acid/disodium hydrogen phosphate buffer.) Related to Figure 2.

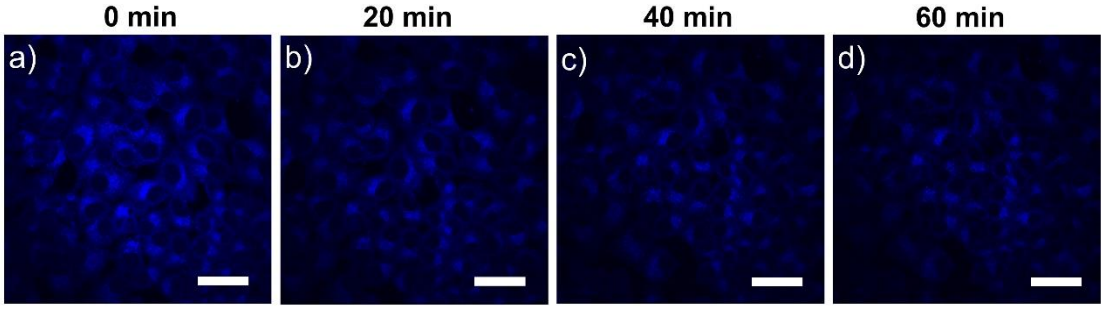

Figure S12. Confocal fluorescence images of A549 cells incubated with CA/oPD-CPDs without treated with dexamethasone. Scale bar: 40 μm. Related to Figure 3.

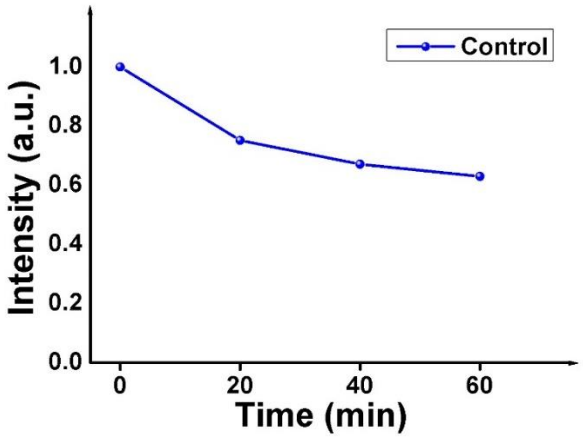

Figure S13. PL intensity of A549 cells incubated with CA/oPD-CPDs without treated with dexamethasone. Related to Figure 3.

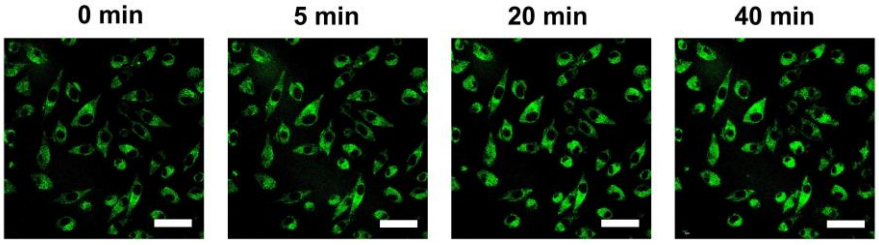

Figure S14. Confocal fluorescence images of living L929 cells incubated with CA/oPD-CPDs under 488 nm laser exposure. Scale bar: 40 μm. Related to Figure 4.

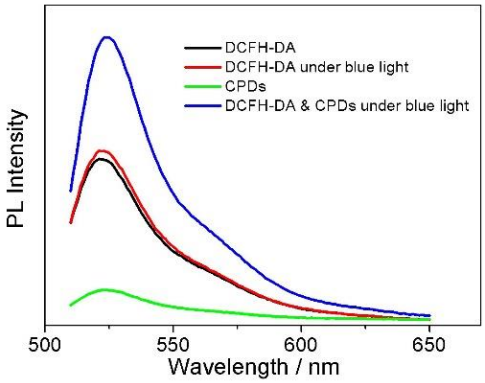

Figure S15. PL spectra of DCFH-DA, DCFH-DA under blue light, CPDs, DCFH-DA with CPDs under blue light. Related to Figure 4.

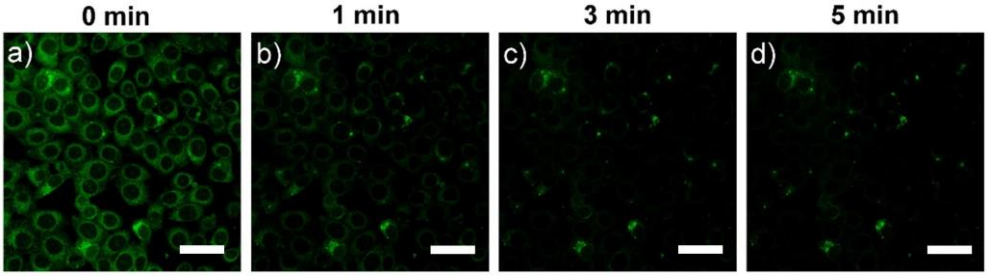

Figure S16. Confocal fluorescence images of fixed A549 cells incubated with CA/oPD-CPDs under 488 nm laser exposure. Scale bar: 40 μm. Related to Figure 4.

Transparent Methods

1. Materials.

Citric acid (99.5%) and o-phenylenediamine (98%) were purchased from Aladdin. Lithium hydroxide monohydrate (90%) was purchased from Beijing reagent. Urea (99%) was purchased from Macklin. Lyso-Tracker Red DND99 was purchased from Invitrogen. Dexamethasone was purchased from Maclin. Human non-small cell lung cancer cell lines A549 and mouse-derived fibroblast cells L929 were purchased from the Academy of Sciences Cell Bank. RPMI medium was purchased from HyClone. Fetal bovine serum and penicillin-streptomycin solution were purchased from Gibco. The Cell Counting Kit-8, CCK-8, was purchased from Dojindo. Cellulose (cotton linter pulp) was supplied by Hubei Chemical Fiber Group Ltd. (Xiangfan, China). Cellulose ester ultra-filtration membranes (0.22 μm) were purchased from Tianjin Navigator Lab Instrument Co., Ltd. Dialysis Membrane (MWCO: 3500 D) are biotech CE tubing and purchased from Spectra/Por Dialysis Membrane. 2',7'-dichlorofluorescein (DCFH-DA) was purchased from Biyuntian Company. All chemicals were purchased and used without further purification.

2. Preparation of CA/oPD-CPDs.

The basic procedures to synthesize CA/oPD-CPDs include two sequential steps in terms of the decomposition and pyrolysis of the mixture of citric acid and o-phenylenediamine. 0.192 g citric acid and 0.108 g o-phenylenediamine were dissolved in the mixture of 10 mL deionized water and 100 μL concentrated hydrochloric acid. The acquired solution was transferred into a poly (tetrafluoroethylene) (Teflon)-lined autoclave (25 mL) and heated at 200 ℃ for 8 h. Then the reactor was cooled to room temperature naturally. The obtained solution was filtrated with ultra-filtration membrane (0.22 μm) to remove larger particles. After filtration, the solution was neutralized with sodium hydroxide, and then centrifuged at 8,000 rpm. The supernatant and the sediment were separately collected. The sediment was transferred to a dialysis bag (3500 D) to remove the remained small molecules for two days in deionized water. The amount of deionized water was 800 mL and the water was changed three times a day. Finally, CA/oPD-CPDs were collected for characterizations and further use. The concentration of CA/oPD-CPDs suspension was determined by the weight of the leftover in 60 ℃ oven per milliliter. The supernatant was purified through column chromatography on silica gel with water as the mobile phase. Batch 2 was the main product and marked as Fluorescent Molecule (FM). Fluorescent Molecule powder was obtained through the freeze-drying process.

3. Cellular toxicity test.

Human lung carcinoma (A549) cells at an initial density of 5×10^3 cells per well were inoculated into the sterile 96-wells plate at 37 ℃ in a humidified 5% CO_2 atmosphere for 24 hours, respectively. Then the culture medium was replaced by a fresh medium with different concentrations of CA/oPD-CPDs (0, 10, 20, 25, 30, 40, 50 μg/mL) and the cells were further incubated for 24 hours. Finally, the samples were washed with PBS, and 100 μL fresh medium with 10 μL CCK-8 was added to each cell well, following by 2 h incubation. A CCK-8 assay was used to analyze cell viability. The optical density was measured at 450 nm. Every condition was repeated for 5 times to gain accurate cytotoxicity data. For the

cytotoxicity of CA/oPD-CPDs with blue light, concentrations of 25 and 50 μg/mL were chosen as typical conditions. To amplify the influence of light exposure, 15 W high powder were applied as long as 2 hours. Without light exposure, the viabilities of cells were 91% (STDEV: 10%) and 79% (STDEV: 16%) when the concentrations were 25 and 50 μg/mL. With blue light exposure, most of A549 cells died. Specifically, the viabilities of cells were 21% (STDEV: 0.18 %) and 17% (STDEV: 0.09%) when the concentrations were 25 and 50 μg/mL.

4. Lysosomes imaging.

Human lung carcinoma (A549) cells were selected for lysosomes bioimaging. A549 cells at an initial density of 2×10^5 cells per well were cultured on a confocal dish for 24 h. Then the cells were incubated with CA/oPD-CPDs with a concentration of 25 μg/mL in a culture medium at 37 ℃ and a humidified 5% CO_2 atmosphere for 24 h. After that, the cells were washed with PBS and further incubated with 100 nM Lyso-Tracker Red DND99 to co-stain the lysosomes in cells for 30 min. After washing and fixing with 2.5% glutaraldehyde for 15 min, the cells were monitored by confocal microscope.

5. Bioimaging of CA/oPD-CPDs during apoptosis.

A549 cells at an initial density of 2×10^5 cells were cultured on a confocal dish overnight. Then the cells were incubated with CA/oPD-CPDs with a concentration of 25 μg/mL for 24 h. After that, 2 μM dexamethasone was added to the culture medium to induce apoptosis and further intracellular pH vibration.

6. Preparation of the composites of CA/oPD-CPDs &cellulose.

As reported in the literature (Wang et al., 2014), 2.4 g LiOH and 4.5 g urea were dissolved in 21.75 mL deionized water. 1.35 g cellulose and 0.2 mg CA/oPD-CPDs were dispersed in the prepared aqueous solution. The whole solution was kept in liquid nitrogen with vigorous stirring until the solution was clear and then centrifuged at 8,000 rpm to degas. The mixture was poured into the designed moulds, and heated at 60 ℃ for 5 hours. The obtained hydrogel was then soaked in deionized water to remove the excess urea and LiOH.

7. Detection of reactive oxidative species.

The ROS detection was evaluated by the DCFH-DA fluorescent probe. Specifically, 12.5 μL of DCFH-DA was added in 0.5 mL of DMSO and then mixed with 2 mL 0.01 mol L^{-1} NaOH under dark condition. After thirty minutes, the reaction was terminated with 10 mL phosphate buffer (25 mM, pH = 7.2) and DCFH-DA solution was achieved. The four groups were set: control (DCFH-DA solution 1 mL with 1 mL DI water), control with blue light exposure, CA/oPD-CPDs aqueous solution (2 mL DI water with 100 μL 2 mg mL^{-1} CA/oPD-CPDs), and DCFH-DA with CA/oPD-CPDs under blue light exposure (DCFH-DA solution 1 mL with 1 mL DI water and 100 μL 2 mg mL^{-1} CA/oPD-CPDs). Blue light exposure was set as 4 W for 5 min.

8. Characterization.

TEM was conducted using a Hitachi H-800 electron microscope at an acceleration voltage of

200 kV with a CCD cinema. Fluorescence spectroscopy was performed with a Shimadzu RF-5301 PC spectrophotometer. The laser confocal microscopy images were obtained with laser scanning confocal microscope OLYMPUS BX81 (FluoView FV1000). UV-vis absorption spectra were obtained using a Shimadzu 3100 UV-vis spectrophotometer. IR spectra were taken on a Nicolet AVATAR 360 FT-IR spectrophotometer. Absolute QY was measured on a fluorescence lifetime and steady-state spectrometer (Edinburgh Instrument, FLS 920, with an integrating sphere). Raman spectroscopy was done by a LabRAM ARAMIS™ Smart Raman spectrometer (Thermofisher) with a He Ne laser at an excitation wavelength of 785 nm. X-ray Photoelectron Spectroscopy (XPS) was investigated by using ESCALAB 250 spectrometer with a mono X-Ray source Al Kα excitation (1486.6 eV). Binding energy calibration was based on C1s at 284.6 eV.

SUPPLEMENTAL REFERENCE

Wang, Z., Fan, X., He, M., Chen, Z., Wang, Y., Ye, Q., Zhang, H., and Zhang, L. (2014). Construction of cellulose-phosphor hybrid hydrogels and their application for bioimaging. J. Mater. Chem. B *2*, 7559-7566.